Representative volume elements for the simulation of isotropic composites highly filled with monosized spheres

Foucault de Francqueville, Pierre Gilormini, Julie Diani

Representative volume elements for the simulation of isotropic composites highly filled with monosized spheres

Foucault de Francqueville[a,b,*], Pierre Gilormini[c], Julie Diani[a]

[a] *Laboratoire de Mécanique des Solides, CNRS UMR 7649, École Polytechnique, ParisTech, 91128 Palaiseau, France*
[b] *ArianeGroup, Centre de recherche du Bouchet, 9 rue Lavoisier, 91710 Vert-le-Petit, France*
[c] *Laboratoire PIMM, ENSAM, CNRS, CNAM, 151 bd de l'Hôpital, 75013 Paris, France*

Abstract

A method is proposed for generating reliable representative volume elements (RVEs) that allows reducing the statistical analysis required for the simulation of the mechanical behavior of isotropic composites highly filled with monosized spheres. The method combines (i) an algorithm inspired from molecular dynamics and associated with an analytical equation of state, and (ii) a geometrical analysis using the two-point correlation function and a nearest-neighbor distribution function. A restrictive selection process is defined, which leads to microstructures reasonably close to randomness and isotropy. The pertinence of the proposed generation and selection of RVEs is confirmed by the simulation of their elastic behavior with the finite element method. In particular, it is shown how the selection procedure allows reducing the computational effort required to reach reliable elastic moduli by operating on a limited number of suitable RVEs. The results are in good agreement with the generalized self-consistent model and with original experimental data obtained on a composite where an acrylate matrix was reinforced by sifted glass beads.

Keywords: Micro-mechanics, Particulate media, Finite elements, Representative volume element

*Corresponding author. Tel. : + 33 1 69 33 57 93
Email address: foucault.de-francqueville@polytechnique.edu (Foucault de Francqueville)

1. Introduction

In order to run numerical simulations, accounting for the local properties and microstructure, of materials highly filled with particles (above 50%) such as propellants, a first step lies in generating representative isotropic random microstructures. In the case of monosized spherical particles, several methods have been designed to generate random microstructures without any one winning over (Bargmann et al., 2018). Microstructures extractions from tomographies or other imaging techniques may be used for their actual representation of the composites (Louis and Gokhale, 1995; Buffière et al., 2008; Maire et al., 2003; Tariel et al., 2011). However they might induce some segmentation complications or restrain the applicable numerical boundary conditions. The random sequential addition (RSA) procedure (Widom, 1966), where particles are randomly and sequentially dispersed in a cell without overlapping, is often adopted (Böhm et al. (2002); Williams and Philipse (2003), for instance). This scheme is limited to spheres volume fractions below 38% due to the frozen position of each particle (Cooper, 1988). Therefore, alternative approaches have also been developed such as rate-dependent densification algorithm (Jodrey and Tory, 1985) or "drop and roll" algorithm (Visscher and M. Bolsterli, 1972) which are rather dedicated to analysis of spheres close packing (Torquato et al., 2000). A more recent approach suggests to start from a Poisson distribution of spheres and exploit an optimization formulation to improve particle localization while enforcing a non-overlapping constraint (Pathan et al., 2017). However the final volume fraction reached hardly exceeds 40%. A Monte Carlo methods allows reaching higher volume fractions (Tobochnik and Chapin, 1988). It is based on the random perturbation of the spheres positions, from an initial microstructure that is periodic usually, enforcing the impenetrability of particles. Optimizing and restraining the interval of perturbations ensure the equilibrium of the final microstructure. Such an approach is known as the Metropolis algorithm (Metropolis et al., 1953; Torquato, 2002). While up to 72% volume fractions of particles may be reached this way, the randomness of highly filled microstructures is questionable (Rintoul and Torquato, 1996), and combined approaches have been developed by mixing the previous methods. The modified RSA scheme, for instance, starts with a low volume fraction RSA microstructure in a cell where particles are submitted to random motions. The particles volume fraction is then increased by incrementally reducing the cell volume (Gusev, 1997; Segurado and Llorca, 2002;

Bailakanavar et al., 2014; Gusev, 2016). Alternatively, the cell size can be kept fixed but the particles radius is increased while they undergo a Brownian motion, modeling molecular dynamics (Lubachevsky and Stillinger, 1990; Skoge et al., 2006; Ghossein and Levesque, 2012). Combination of this latter method with Montecarlo steps (shaking process) has also been envisioned (Buryachenko et al., 2012) but the molecular dynamics approach is retained here because an implementation is directly available where the pressure induced in the cell during the process is computed, which provides very useful information.

Once a microstructure has been generated, its linear elasticity can be estimated to assess its potential as representative volume elements (RVEs) of the composite material (Huet, 1990; Hazanov and Huet, 1994; Gusev, 1997; Kanit et al., 2003; Ghossein and Levesque, 2012; Garboczi and Kushch, 2015). Characterizations of the geometry of the microstructures can also be performed (Rintoul and Torquato, 1996, 1998), and complement the former analysis. The concept of the present approach is to explore the ability of the generating presure, the two-point correlation function and various nearest-neighbor distribution functions (Torquato, 2002) to efficiently help selecting the more random and isotropic microstructures (Chiu et al., 2013). Applying such a preselection is arguably uninteresting when dealing only with the linear mechanical responses. Nonetheless, it becomes hard to avoid when running finite elements analyses dealing with nonlinear behavior or with cohesive interfaces (Park and Paulino, 2011). Understanding the statistical discrepancy when considering relatively small RVEs, our goal is to reduce the number of numerical microstructures required to still reach accurate estimates of the material mechanical response, and linear elasticity is used only to validate the preselection. Some recent studies (Segurado and Llorca, 2002; Gusev, 2016) consider spheres volume fractions over 50% and compare finite element results to the differential model (McLaughlin, 1977), the Torquato model (Torquato, 1998, 1991), or the generalized self-consistent model (GSC) (Christensen and Lo, 1979; Christensen, 1990). Since quantitative comparison with experimental data is scarce in the literature, a model composite made of a rubbery matrix highly filled with sifted glass beads was prepared and tested in uniaxial tension in the present study. This was already the case in the work of Gilormini et al. (2017), where a finite element analysis (FEA) was applied to a single microstructure generated through a much simpler and less validated procedure than here.

The paper is organized as follows. In the next section, an algorithm gen-

erating microstructures is described. The impact of its seed parameters in regards of the resulting microtructures and geometries is presented. Based on the requirement of isotropic mechanical properties, a selection procedure is defined in Section 3 from the finite element analysis of the microstructures, including a careful mesh refinement. Finally, the obtained numerical properties are confronted to homogenization models and to original experimental data in Section 4.

2. Microstructures highly and randomly filled with monosized spheres

2.1. Random cell generation

The Lubachevsky and Stillinger (1990) approach is applied here to generate microstructures. A detailed example of implementation is availaible in Ghossein and Levesque (2012), and an other version of the algorithm, developed by S. Torquato and his coworkers (Skoge et al., 2006), is available for download on the website of this author. First, a classical RSA algorithm is applied to disperse a low volume fraction of monosized spheres randomly in a periodic cubic cell. Then, an initial velocity $\mathbf{v}$ is given to each particle according to a Maxwell-Boltzmann distribution:

$$f(\mathbf{v}) = \left(\frac{m}{2\pi k_B T}\right)^{3/2} \exp\left(-m\frac{\mathbf{v}.\mathbf{v}}{2k_B T}\right) \tag{1}$$

where all particles have the same normalized mass $m = 1$, k_B is the Boltzmann constant, and the only parameter driving the distribution of velocities is the thermodynamic temperature T. To reach the desired high volume fraction, a growing factor g_{fact} is applied to all spheres while their mass is kept constant, resulting in an unaffected distribution of velocities. Due to the growing spheres size, the probability of collision between moving spheres increases, and an event-driven process is defined (Lubachevsky and Stillinger, 1990), where all velocities are decreased uniformly after a given number of events reducing the risks of two simultaneous collisions that would stop the algorithm. Applying the latter constraint also lowers the risk of strong pressure divergence (this phenomenon will be discussed in Section 2.3 below) that may prevent reaching the expected volume fraction. Examples of configurations obtained during a cell generation are presented in Figure 1 with specification of the main generating parameters: temperature T and growing factor g_{fact}.

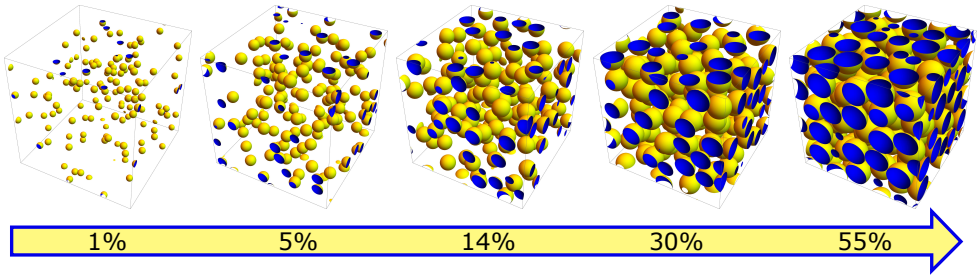

Figure 1: Examples of microstructures obtained at various intermediate volume fractions during a microstructure generation with a mixed method combining an initial RSA scheme and particles velocities and growth defined by parameters $T = 0.2$ and $g_{fact} = 0.005$.

2.2. Geometrical analysis

In accordance with the literature (Gusev, 1997; Ghossein and Levesque, 2012; Gusev, 2016), elementary periodic cells containing 64 spheres of equal diameters were generated (Chiu et al., 2013). A microstructure can be analyzed by computing various geometrical characterization functions, but only few of them lead to usable results here for the relatively small number of spheres (Torquato, 2002). Nonetheless, the two-point correlation function S_2 and some nearest-neighbor distribution functions have revealed interesting properties to detect poor randomness. Since reference values have been estimated theoretically by Torquato et al. (1990) based on Reiss et al. (1959), the neighbor distribution functions H_v that characterizes the distance from every point of the matrix to the closest sphere centers, is chosen.

The S_2 function is a common tool for a first characterization of randomness (Lee et al., 2011; Chiu et al., 2013). In the present context, its evaluation will focus on the reinforcement phase and will therefore be defined as the probability for a vector $\mathbf{r}$ with its origin, orientation and length chosen randomly to have both its origin and end located in the particle phase, taking the cell periodicity into account. A classical procedure based on fast Fourier transform, recalled in appendix A (Ohser and Schladitz, 2009), was implemented as a Matlab (Matlab, 2016) routine.

Figure 2 illustrates the S_2 values obtained when 55% volume fraction of spheres are either organized as a BCC lattice (Figure 2a) or disordered according to a Percus-Yevick (Percus and Yevick, 1958) random distribution (Figure 2b). Note that the later is a rather close representation of a perfect random distribution at the considered volume fractions (Katzav et al.,

2017). Both figures, where r_1/D, r_2/D and r_3/D denote the components of the sampling vector normalized by the spheres diameter D, show the S_2 values computed in the three coordinate planes of one eighth (because of periodicity and parity of the S_2 function) of the cell. While usual analyses are restrained to few directions, uncommon 2D plots are proposed here as extensive samples of the full 3D sets of S_2 values given by the above numerical procedure. Circular lines, which correspond to $|\mathbf{r}|/D = 1, 2, 3, ...$, are also plotted to help the eyes recognizing the isotropy symmetry. In Figure 2a, the crystallographic BCC arrangement in the cell is clearly revealed by the periodic variations of the S_2 function. In contrast, the S_2 values in Figure 2b, computed from the results tabulated by Torquato and Stell (1985) for the Percus-Yevick distribution, obey a spherical symmetry that reveals isotropy. In Figures 2a and 2b, the S_2 value at the origin of the axes is the volume fraction of spheres (η), as it stands for the probability for a point chosen randomly (i.e., a zero-length sampling vector) to lie in a reinforcement. In addition, as soon as sampling vectors growth in Figure 2b, S_2 reaches values close to this fraction squared (η^2) which denotes a large range of test vectors with decorrelation at their origin and end, as should apply in a perfectly random distribution. Figure 3b shows the S_2 values obtained from the tomographic analysis of a composite material that has been prepared by randomly mixing a volume fraction of nearly 55% of sifted glass beads in a rubbery matrix (Figure 3a). This experimental two-point correlation function exhibit the same features as displayed in Figure 2b, which is in favor of a fairly random and isotropic distribution of reinforcements for the actual composite.

2.3. Pressure evolution

The selected generation algorithm provides with an estimate of the reduced pressure p during spheres growth. The latter is obtained by calculating the Clausius virial function and normalized it with the perfect gas pressure ($P_{gas} = nk_BT/V$, where n is the number of particles and V the volume)

$$p = 1 + \frac{1}{2E_c} \left\langle \sum_{i=1}^{n} \mathbf{r}_i \cdot \mathbf{F}_i^{Int} \right\rangle, \tag{2}$$

where the expression of the Boltzmann kinetic energy $E_c = 3nk_BT/2$ has been used and brackets correspond to time averaging. Since the only potential considered during the microstructure generation process is the interaction

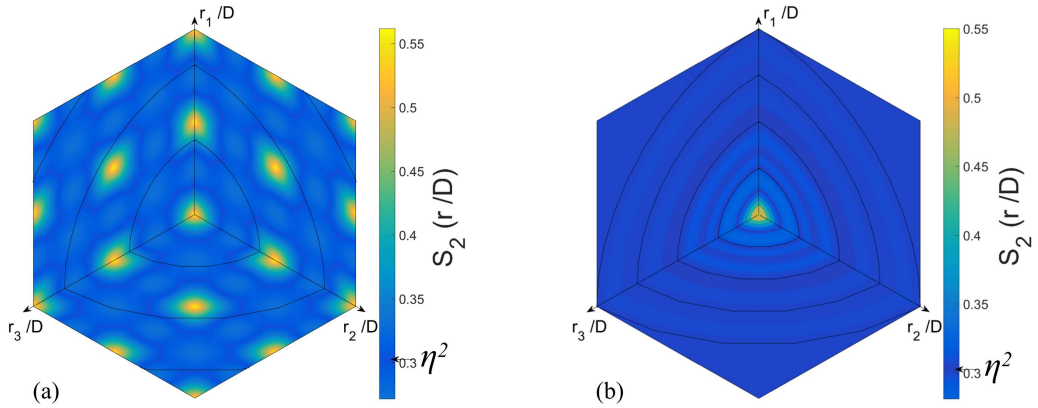

Figure 2: Maps of the two-point correlation function S_2 for various microstructures at 55% volume fraction for (a) a perfectly ordered microstructure and (b) a Percus-Yevick random microstructure.

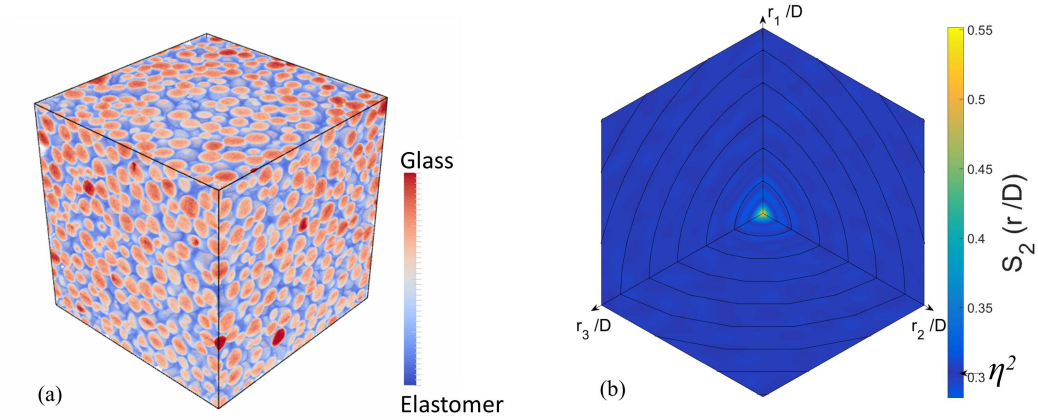

Figure 3: Experimental microstructure obtained by X-Ray tomography analysis (a) and the corresponding two-point correlation function (b). The composite is made of a 55% volume fraction of glass beads dispersed randomly in an elastomeric matrix.

between colliding particles (Skoge et al., 2006), the scalar product of sphere position $\mathbf{r}_i$ with internal force $\mathbf{F}_i^{Int}$ can be estimated from the momentum X_m exchanged by particles collisions during duration Δt,

$$p = 1 + \frac{X_m}{2E_c\,\Delta t}. \tag{3}$$

The pressure in systems of randomly dispersed monosized hard spheres has already been addressed theoretically, and several equations of states (EOS) have been proposed for its evolution with the particles volume fraction η. The Carnahan-Starling-Kolafa model (Boublík and Nezbeda, 1986), as expressed by Robles et al. (2014), is used here:

$$p = \frac{1 + \eta + \eta^2 - \frac{2}{3}\,(1+\eta)\,\eta^3}{(1-\eta)^3}. \tag{4}$$

Figure 4 shows the evolution that can be obtained for three representative microstructures, depending on the parameters used in the generation process (see Section 2.1). An atypical confrontation to their corresponding geometrical properties is performed. First, a pressure drop may be observed for low values of the g_{fact}/T ratio. The S_2 values for the corresponding microstructures have similarities with the ordered case of Figure 2a, suggesting that some crystallization happened during the generation process (Hoover and Ree, 1968). This result is confirmed by the nearest-neighbor distribution function, which diverges from the reference defined for a random microstructure. This phenomenon is explained by a drop of the number of reachable random states above a 'freezing point' at about 49.4% volume fraction, when the system tends to order (Rintoul and Torquato, 1996). Figure 4 illustrates also that a divergent pressure evolution may appear if the g_{fact}/T ratio is too large. The corresponding microstructures have S_2 values close to the distribution of Figure 2b, but their nearest-neighbor distribution functions differ from the reference for a random distribution, suggesting a particles clustering consistent with the sudden increase of the number of collisions. Finally, when intermediate values of g_{fact}/T are used, the pressure follows the EOS closely, and some of the obtained microstructures are found satisfactory in terms of both S_2 and $\mathrm{H_v}$. Therefore, the two main parameters of the generation process must be balanced carefully in order to ensure a pressure evolution close to the EOS, and random microstructures may be expected after the geometrical analysis is applied.

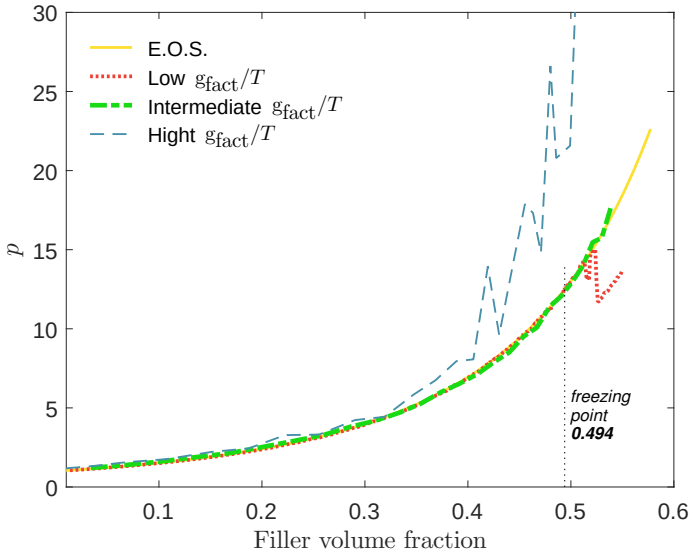

Figure 4: Three types of reduced-pressure evolutions for various g_{fact}/T ratios, compared to the Carnahan-Starling-Kolafa equation of state.

3. Tests of the microstructures isotropy by finite element analysis

3.1. FEA framework

The generated microstructures are meshed in order to calculate their elastic properties by FEA and to recognize the less anisotropic microstructures as reasonnable RVEs. The Netgen free meshing software (Schberl, 1997; Schneider et al., 2016) conveniently generates periodic meshes and lists the periodic displacement constraints to be used by the finite element code Abaqus (2014). Most FEAs of monosized spheres systems previously performed in the literature (Gusev, 1997; Segurado and Llorca, 2002; Barello and Levesque, 2008) were based on RVEs with limited minimum interparticle distances (δ) for improving the mesh quality. However, Gusev (2016) noticed recently that the mechanical properties are underestimated when large interparticle distances are imposed, typically $\delta/D > 10^{-3}$. To avoid interparticle distance restrictions without introducing distorted elements, the mesh is refined where spheres are very close (Figure 5). For any given pair of close particles, a set of circles of latitudes is defined around the pole at the point closest to the other sphere. Several points are uniformly distributed on these circles to

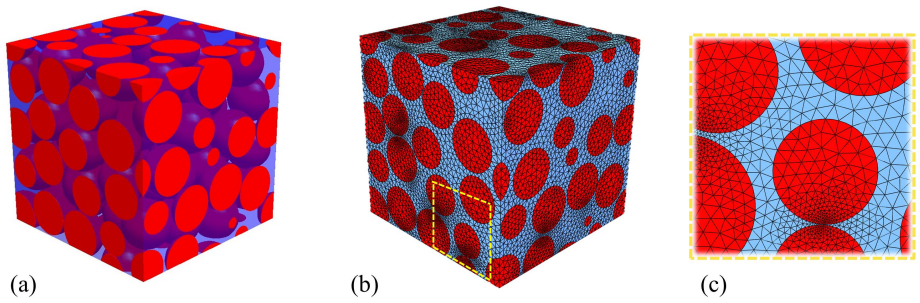

Figure 5: (a) A generated microstructure. (b) Its discretization using the meshing procedure. (c) Enlarged view illustrating the local mesh refinement.

reduce the element size ensuring a high quality mesh. Although the refinement induces a significant increase of the number of degree of freedom, the computational duration is shortened. For discretizations with C3D10 tetrahedra, one million elements are generated typically, with five millions degree of freedom. Such a method allows automatic and robust meshing of the microstructures without user input, therefore it can be operated for systematic analyses as easily as the technique based on fast Fourier transform (Moulinec and Suquet, 1998) which is classically preferred for its straightforwardness (Ghossein and Levesque, 2012; Dunant et al., 2013). FEA is adopted in the present contribution for its proven flexibility to explore further features of the composite such as finite strain, viscoelasticity and interface debounding (Park and Paulino, 2011).

Highly contrasted phases with small-strain linear elastic behaviors are considered in the following numerical applications. The composite consists of an incompressible soft matrix with a Young modulus of 6 MPa filled with hard particles with a Young modulus of 69 GPa and a Poisson's ratio of 0.25. Hybrid elements are used in the incompressible matrix phase. Note that the impact of the matrix properties will also be tested by increasing its stiffness and compressibility in Section 4. A perfect adhesion is assumed at the filler-matrix interface and periodic boundary conditions are applied to the cubic cell. When run on eight cluster nodes (2.5 GHz Intel Xeon E5-2640 CPU, 64 GB RAM), the simulation of one uniaxial tensile test requires approximately one hour. In order to test the isotropy of the composite, each microstructure is submitted to six loadings consisting in either a uniaxial tension or a simple shear along a cell axis, so that three Young moduli (E_1, E_2, E_3) and three shear modului (μ_1, μ_2, μ_3) are obtained. The lowest

dispersions for each set of moduli are expected to select the less anisotropic microstructures. Moreover, an additional and original criterion for isotropy is proposed when an incompressible soft matrix is considered: because of the incompressible overall behavior of the composite due to an incompressible matrix and comparatively rigid inclusions, in addition to $E_1 = E_2 = E_3$ and $\mu_1 = \mu_2 = \mu_3$, the ratio $\overline{E}/3\overline{\mu}$, where $\overline{E} = (E_1+E_2+E_3)/3$ and $\overline{\mu} = (\mu_1+\mu_2+\mu_3)/3$, should be exactly equal to 1 for a perfectly isotropic composite. While perfect isotropy is unrealistic for the present microstructures, this test reject ordered microstructure with cubic symmetry where the equalities between moduli apply although $\overline{E}/3\overline{\mu}$ differs from 1.

3.2. Statistical Analysis

Twenty different microstructures containing a 55% volume fraction of spheres have been built with generation parameters providing cell pressure evolutions in good agreement with the EOS (see Section 2.3). Their elastic behaviors have been computed and are presented in Figure 6 in terms of the three Young moduli and shear moduli normalized by the respective matrix values, and the additional isotropy criterion computed as $\left|\overline{E}/3\overline{\mu} - 1\right|$. The whole generation process was repeated for each microstructure, starting from a different RSA distribution, so that the number identifying each microstructure is arbitrary and on te figure each color stand for the properties of one realization. One notes in Figure 6 that all microstructures do not perform equally. For instance, microstructure 6 presents low dispersions of Young moduli and shear moduli, with averages close to the values estimated over the twenty microstructures, and a very good value for the isotropy criterion. In contrast, microstructure 7 exhibits a small dispersion of Young modulus but a large dispersion of shear modulus, with a poor value for the isotropy criterion. Therefore, the following question arises: instead of running FEAs on every generated microstructures, can geometrical analyses be used preliminarily to select fewer microstructures to which FEA is worth being applied? Such a procedure might not be crucial for elastic behaviors, but it might become mandatory when finite strain, interfacial damage, or viscoelasticity, for instance, are considered, because of long computation durations.

Consequently, the geometrical analysis described in 2.2 has been applied to each of the above 20 microstructures, in order to show ability to reject the cases where unsatisfactory mechanical properties could have been expected before running FEA. In order to illustrate the results, we will focus on four microstructures, which are representative of the features that can be

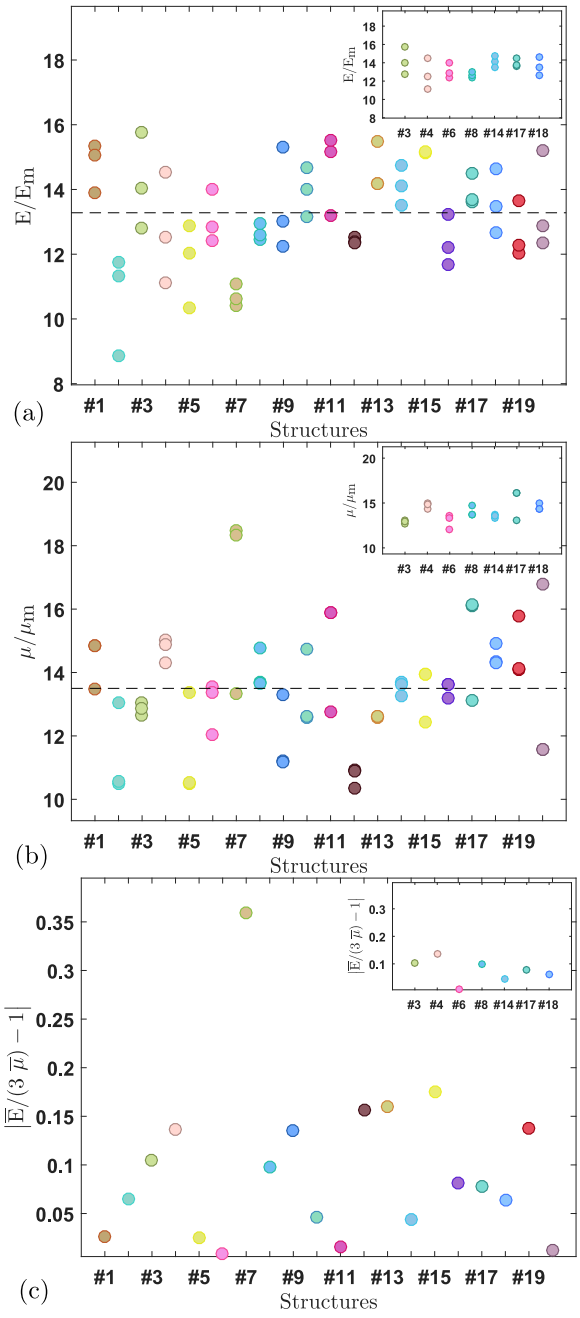

Figure 6: Values of the Young modulus (a) and shear modulus (b) obtained in the directions of the three cell axes and normalized by the matrix values for 20 microstructures. Isotropy criterion (c) calculated with the average Young modulus and average shear modulus for each microstructure. Insets correspond to the same data but considering only the 7 selected microstructures

obtained. Microstructure number 6 presents a reasonable randomness while numbers 2, 7 and 11 are examples of microstructures that should be discarded before being meshed (See Figure 6). Figure 7 presents the S_2 values for these four microstructures, with a reduced color scale centered on the asymptotic value (η^2). Microstructures 2 and 7 can be discarded readily as they do not exhibit any asymptotic trend and as their dispersed peaks are inconsistent with a symmetric evolution of S_2. In contrast, microstructures 6 and 11 present S_2 values with features similar to the reference displayed in Figure 2b, meaning spherical symmetry of S_2 and convergence to η^2 for long test vectors, which suggests promising randomness and isotropy. As a further test, Figure 8 compares the nearest-neighbor distribution function $\mathrm{H_v}$ computed on microstructures 6 and 11 to the perfect random reference described in 2.2 (Reiss et al., 1959). This comparison allows rejecting microstructure 11 while microstructure 6 shows the best randomness from the nearest neighbor point of view. Considering all 20 microstructures, we have noticed that every microstructure presenting non-negligible anisotropic shows either a poor S_2 periodicity or unsatisfactory nearest neighbor distribution. Therefore, S_2 and $\mathrm{H_v}$ characterizations provide efficient tools to discard undesired anisotropic microstructures.

The mechanical properties of the seven microstructures selected (namely, microstructures number 3, 4, 6, 8, 14, 17, and 18) are reported in the insets of Figure 6, highlighting the reduction of the moduli dispersions by a factor of nearly 2 and the exclusion of microstructures with unsatisfactory values for the isotropy criterion. It may be noted that averaging the Young modulus and the shear modulus over the seven final microstructures leads to values (80.9 MPa and 27.9 MPa, respectively) similar to the averages computed over the twenty generated microstructures. Two thirds of the computational effort involved in meshing and finite element simulations would have been avoided by applying the geometrical analysis right after microstructures generation. The remaining fluctuations in the insets of Figure 6 (standard deviations of 10.2% for the Young modulus and 7.3% for the shear modulus) highlight the unfeasibility of generating perfectly isotropic microstructures with such a few number of particles and periodicity justifying the requirement for a statistical approach. Convergence is finally facilitated when, despite studying all the generated realizations, the analysis is retrained to the most representatives microstructures, that can be considered as RVEs.

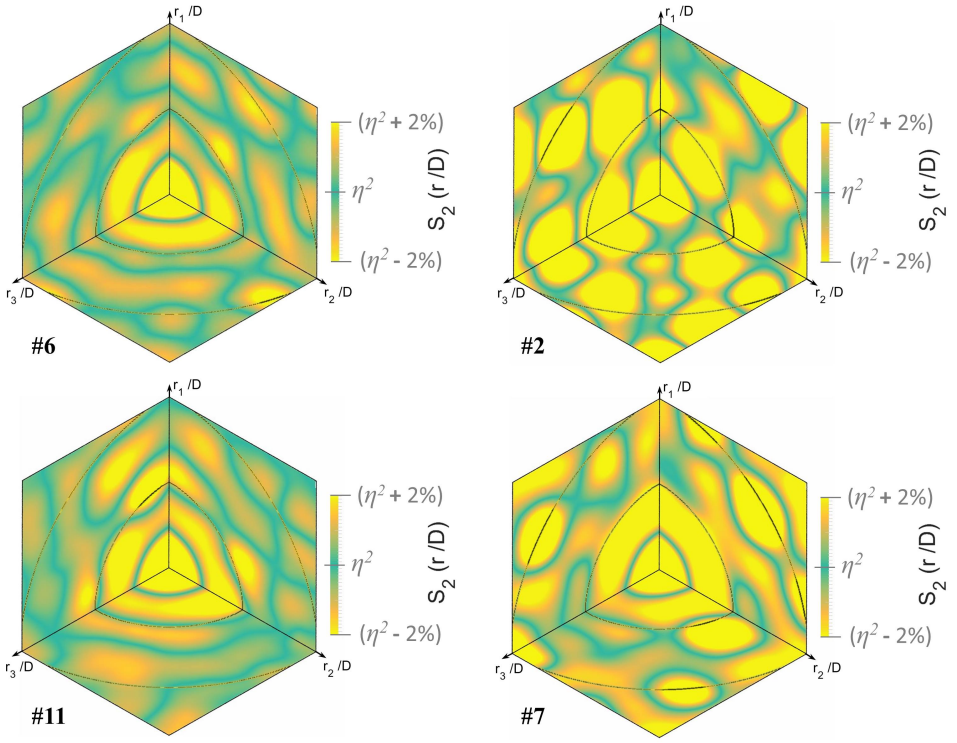

Figure 7: S_2 values for typical microstructures with a reduced color scale centered on η^2. Solid lines are guides for eyes to estimate spherical symmetry. Spherical trend of the left diagrams clearly differ from dissipated peaks of the right ones.

4. Representativeness of the selected RVEs

The elastic moduli obtained by FEA on the set of selected RVEs are now compared to the predictions of mean field homogenization models, to FEA results taken from the literature, and to original experimental data measured on a rubbery acrylate network filled with sifted glass beads.

In the case of an incompressible matrix filled with a 55% volume fraction of glass beads, the shear moduli given by the FEA simulations compare very favorably to the predictions of the GSC model (Christensen and Lo, 1979; Christensen, 1990) for a wide range of matrix Young modulus E_m values, as shown in Figure 9a. This result is consistent with recent literature (Gusev, 2016; Ghossein and Levesque, 2012), even when taking into account the reduced uncertainty obtained with the previous selection process, as illustrated

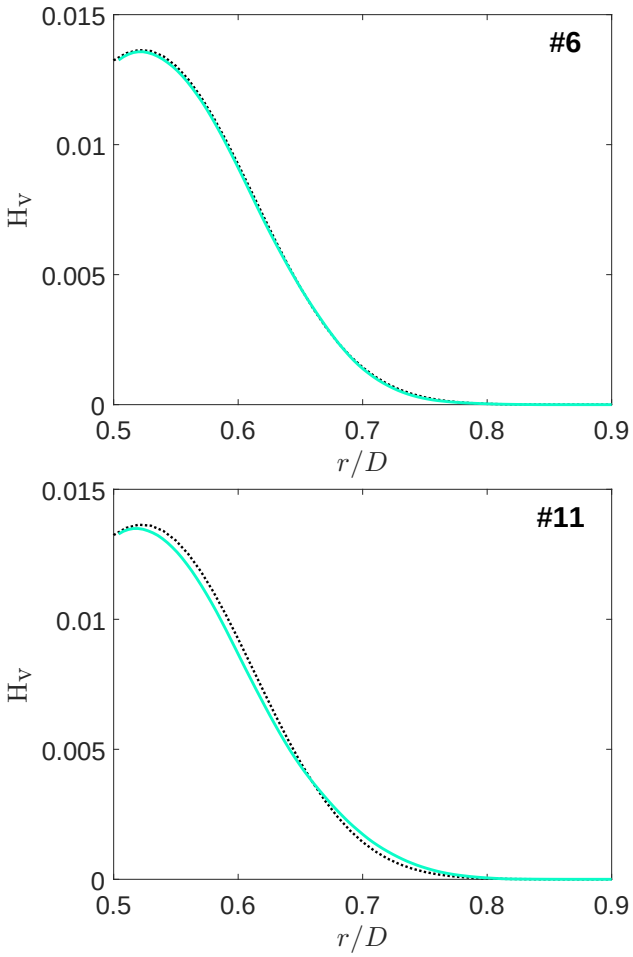

Figure 8: Nearest-neighbor distribution function for microstructures 6 (top) and 11 (bottom). The dotted line is the reference function.

for $E_m = 6$ MPa. It should be noted that the predictions of the Torquato model (Torquato, 1991, 1998) and the differential model (McLaughlin, 1977) would lay roughly 50% below the FEA results at such a large volume fraction. In order to complete our analysis, much larger matrix stiffnesses were considered while the matrix Poisson's ratio was lowered to 0.4, in order to model a polymer in the glassy state. As shown in Figure 9b, the coherence between numerical results and the GSC model is more questionable in these conditions.

Comparing a model to other models provides with interesting fundamental outcomes but does not prove its relevance for actual materials. While most of the reference studies restrain their confrontation to homogenization models (Gusev, 2016; Ghossein and Levesque, 2012; Segurado and Llorca, 2002), a composite made of an acrylate polymer network higly filled with sifted glass beads has been prepared and tested. The polymer matrix was obtained by mixing 98% molar mass of methacrylate (MA) with 2% molar mass of polyethylene glycol dimethacrylate (PEGDMA) of molar weight 750 g/mol and adding 2,2-Dimethoxy-2-phenylacetophenone (DMPA) as photo-initiator. This composition was chosen to synthetize a rubbery network at room temperature in order to obtain a composite with a soft and incompressible matrix. Glass beads with diameters ranging from 200 to 250 μm were slowly poured into the acrylate mix, avoiding beads agglomeration and ensuring complete wetting. The compound was poured between two glass plates spaced by a 3 mm teflon frame and maintained vertical during polymer crosslinking in an ultraviolet chamber for 40 minutes. A fairly isotropic distribution of spheres is obtained, as already shown with the tomographic analysis shown in Figure 3. Specimens of $40\times12\times3$ mm^3 were punched at the bottom of the plates to ensure similar glass beads volume fractions in every sample. Moreover, 1 mm-thick plates of pure polymer were also prepared to measure the matrix elastic properties and implement them in the numerical simulations. The composite high volume fraction results from the gravity applying on the beads in a low viscosity uncrosslinked matrix, which prevents any adjustment during the synthesis. Densimetry measures revealed an average density of 52% with a rather small scatter of 1%. Tensile tests at low constant crosshead speed (0.1 mm/min) were carried out, during which the strain was measured by video extensometry (Instron AVE2) and the force by a class 0.5 10 kN cell. Six specimens were tested for the pure acrylate and for the composite, showing good reproducibility. The matrix Young modulus was measured at 5.7 ± 0.5 MPa and the composite Young modulus at

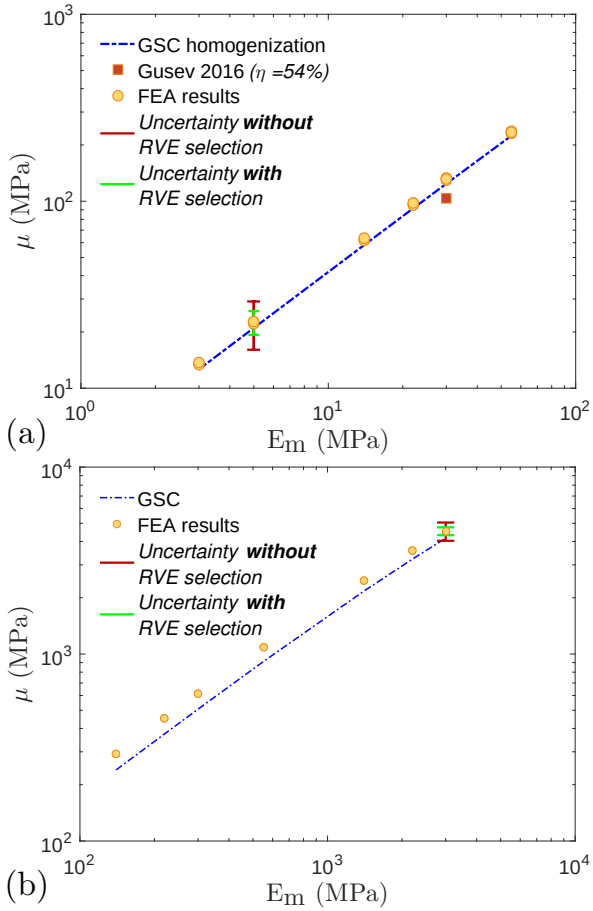

Figure 9: Shear moduli given by the FEA simulations and the GSC model when the polymer matrix (Young modulus E_m) of the composite is either rubbery (a) or glassy (b). The volume fraction of glass beads is 55% and the results without error bars were obtained with microstructure number 6.

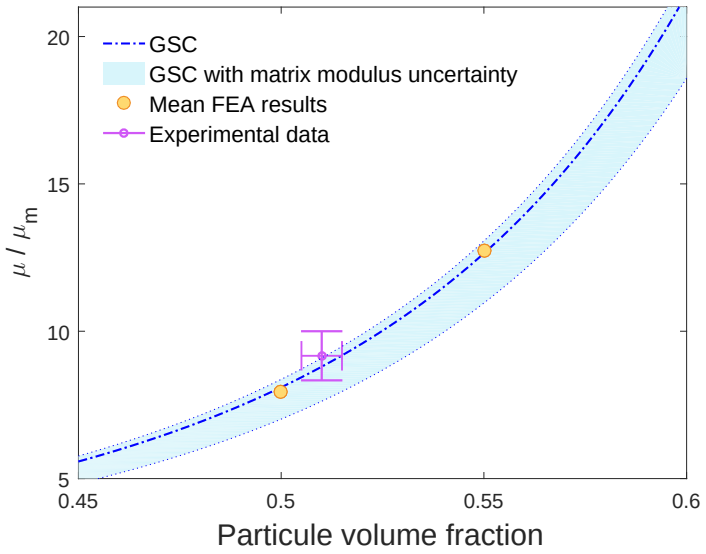

Figure 10: Global consistency between the Young modulus estimated with the FEA simulations (averages over 7 selected microstructures in each case), the GSC model, and measured experimentally.

55 ± 1 MPa. A comparison between the actual composite modulus, including uncertainties on modulus and on volume fraction, and the average FEA results obtained from 7 selected RVEs at volumes fractions of 55% and 50% (for which the generation and selection procedures presented above at 55% have been repeated) is shown in Figure 10. Results given by GSC model are also plotted when accounting for the matrix modulus uncertainty. Both this model and FEA applied to the set of selected RVEs predict very satisfactorily the stiffness of an actual incompressible rubbery polymer matrix filled with monosized glass beads at the high density experimentally obtained.

The present approach has been developed and tested only for monosized spherical particles with a high contrast between the rigid inclusions and the rubbery matrix. Further extensions may be envisioned for more complex fillers as dedicated approximation of the equation of state are available mostly based on the scaled particles theory (Boublík, T., 1974; Reiss, 1992; Allen et al., 1993). This would allow selecting complex microstructures based on the analysis of the generated pressure coupled with the geometric characterization, which is the major originality of the current approach. However particles irregularities require an orientational order analysis in addition to present positioning order examinations. That would be exacerbated when

large aspect ratio particles are considered, which could also induce considerations for a nematic thermodynamic state (Frenkel and Mulder, 1985). Therefore, the natural extension of the present approach to monosized ellipsoid for instance, will require a deep revision of the selection process even if Lubechevsly and Stillinger algorithm for such particles as been already developed (Donev et al., 2005a,b). The pressure-based selection will have to consider nematic states (orientationnal order) in addition to solids state (positional order) and the geometrical characterization will have to include orientation characterization functions. Such extensions are beyond the framework of the present study despite the interests that may arouse for a selection process efficient with complex RVEs.

Another extension would have been analyses of the impact of phases contrast on the relevance of the selection process. Reduction of the contrast has been briefly considered in section 4 without any experimental validation of the numerical estimation of the composite mechanical properties. Studying the inversion of the phase contrast (voids instead of rigid inclusions) might be of particular interest especially for modeling rocks behavior.

5. Conclusion

In this study, a method was proposed for the efficient generation and selection of reliable RVEs that allows reducing of two thirds the statistical analysis required for the numerical simulation of the mechanical behavior of isotropic composites randomly and highly filled with monosized spheres. The method proceeds in two steps. First, an algorithm inspired from molecular dynamics is applied, where spheres collide and grow simultaneously in a periodic cubic cell, starting from an initial RSA distribution at a low volume fraction. The microstructures obtained at high volume fraction are rejected if a reference equation of state is not followed during this process, which allows adjusting the two parameters involved. In a second step, a geometrical analysis is performed to select microstructures further. The two-point correlation function is computed and allows identifying the features expected from random and isotropic microstructures. Finally, a nearest-neighbor distribution function is computed and compared to a reference in order to perform a final selection among the microstructures.

The relevance of the proposed generation and selection of RVEs has been confirmed by the simulation of their elastic behavior with the finite element method, where the mesh was refined carefully. First, the microstructures

selected by the geometrical analysis have been shown to be reasonably close to isotropy in terms of the dispersions of the Young modulus and shear modulus. This was also consistent with the ratio of 3 between these moduli that is expected for isotropic incompressible composites. Moreover, the average moduli obtained from the selected microstructures were found very similar to the averages obtained without applying the geometrical analysis, but with much narrower dispersions. Thus, the proposed selection procedure allows reducing the computational effort required to reach reliable elastic moduli by operating on a limited number of suitable RVEs. This confirms the efficiency of comparing pressure evolution with the EOS and of the considered geometrical functions for a rapid discrimination of the reasonably random and isotropic microstructures. While further morphological characterizations might reduce the number of considered realizations and the properties discrepancies, they will mostly be significantly time consuming or even inoperative due to the cell size.

The numerical results have been confronted to homogenization models, and a very good agreement has been obtained with the generalized self-consistent model, especially when a soft and incompressible matrix contains a large volume fraction of monosized stiff spheres. Very interestingly, a good agreement has also been found with original experimental results obtained on a model composite where a rubbery acrylate matrix was reinforced by sifted glass beads. This contributes to validate the ability of the proposed methodology to predict the elastic behavior of composites with good precision. Keeping the same guidelines, it may also be adapted to nonlinear behaviors, finite strains or damage at matrix-particles interfaces, for instance.

Acknowledgements

The acquisition of the microtomography device of laboratoire Navier (ENPC) has been made possible thanks to grants from the Region Ile de France (SESAME 2007 program) and CNRS. This work was supported by the ANR under contract number ANR-10-EQPX-37 and the authors thank the Délégation Générale de l'Armement (DGA) and ArianeGroup for their financial supports.

Appendix A

A dense set of S_2 values can be computed by letting the origin and end of the sampling vector scan systematically all the nodes of a thin cubic grid,

and the calculation can then take full advantage of the remarkable properties of circulant matrices (see for instance Van Loan (1992), for basic relations between circulant matrices and Fourier transform, and Yongshe et al. (2006) for application to 3D correlation). Practically, we applied the following simple numerical procedure to compute the values of the S_2 function:

(i) The elementary microstructure cubic cell is sampled into a $N \times N \times N$ matrix with a value of 1 for each voxel located in a spherical reinforcement and 0 in the matrix.

(ii) This $N \times N \times N$ matrix of integers is changed into a matrix of complex numbers, where the real part is equal to the integer value (1 or 0) and the imaginary part is zero.

(iii) The discrete 3D Fourier transform of this complex matrix is computed by applying a fast Fourier transform (FFT) algorithm.

(iv) All elements of the resulting $N \times N \times N$ matrix of complex numbers are modified, with their real parts replaced by their moduli squared and their imaginary parts set to zero.

(v) The inverse discrete 3D Fourier transform of this modified matrix is computed by FFT, which leads to a $N \times N \times N$ matrix of complex numbers where the imaginary parts are zero and the real parts are the S_2 values.

It is important to note that a division by N^3 is included in the definition of the discrete 3D Fourier transform used above (but not in the inverse transform, of course), and therefore the division by N^3 involved implicitly in the definition of S_2 (to obtain the average over all locations of the origin of a sampling vector with fixed orientation and length) is performed when the moduli are squared in step (iv) above.

References

Allen, M. P., Evans, G. T., Frenkel, D., Mulder, B. M., 1993. Hard convex body fluids. Adv. Chem. Phys. 86, 1–166.

Abaqus, 2014. Abaqus standard version 6.14. Dassault Systèmes Simulia Corp.

Bailakanavar, M., Liu, Y., Fish, J., Zheng, Y., 2014. Automated modeling of random inclusion composites. Eng. Comp. 30, 609–625.

Barello, R., Levesque, M., 2008. Comparison between the relaxation spectra obtained from homogenization models and finite elements simulation for the same composite. Int. J. Solids Struct. 45, 850–867.

Bargmann, S., Klusemann, B., Markmann, J., Schnabel, J. E., Schneider, K., Soyarslan, C., Wilmers, J., 2018. Generation of 3D representative volume elements for heterogeneous materials: a review. Prog. Mater. Sci. 96, 322–384.

Böhm, H., Eckschlager, A., Han, W., 2002. Multi-inclusion unit cell models for metal matrix composites with randomly oriented discontinuous reinforcements. Comput. Mater. Sci. 25, 42–53.

Boublík, T., 1974. Statistical thermodynamics of convex molecule fluids. Mol. Phys. 27, 1415–1427.

Boublík, T., Nezbeda, I., 1986. P-V-T behaviour of hard body fluids. Theory and experiment. Collect. Czech. Chem. Commun. 51, 2301–2432.

Buffière, J. Y., Cloetens, P., Ludwig, W., Maire, E., Salvo, L., 2008. In situ X-ray tomography studies of microstructural evolution combined with 3D modeling. MRS Bull. 33, 611–619.

Buryachenko, V. A., Jackson, T. L., Amadio, G., 2012.Modeling of random bimodal structures of composites (application to solid propellants): I. Simulation of random packs. Comput. Model. Eng. Sci. 85, 379–416.

Chiu, S. N., Stoyan, D., Kendall, W. S., Mecke, J., 2013. Stochastic geometry and its applications. John Wiley and Sons

Christensen, R., Lo, K., 1979. Solutions for effective shear properties in three phase sphere and cylinder models. J. Mech. Phys. Solids 27, 315–330.

Christensen, R. M., 1990. A critical evaluation for a class of micromechanics models. J. Mech. Phys. Solids 38, 379–404.

Cooper, D. W., 1988. Random-sequential-packing simulations in three dimensions for spheres. Phys. Rev. A 38, 522–524.

Donev, A., Torquato, S., Stillinger, F. H., 2005a. Neighbor list collision-driven molecular dynamics simulation for nonspherical hard particles. I. Algorithmic details. J. Comput. Phys. 202, 737–764.

Donev, A., Torquato, S., Stillinger, F. H., 2005b. Neighbor list collision-driven molecular dynamics simulation for nonspherical hard particles. II. Applications to ellipses and ellipsoids. J. Comput. Phys. 202, 765–793.

Dunant, C. F., Bary, B., Giorla, A. B., Péniguel, C., Sanahuja, J., Toulemonde, C., and Yvonnet, J., 2013. A critical comparison of several numerical methods for computing eective properties of highly heterogeneous materials. Adv Eng Softw, 58, 1–12.

Frenkel, D., Mulder, B. M., 1985. The hard ellipsoid-of-revolution fluid: I. Monte Carlo simulations. Mol. Phys. 55, 1171–1192.

Garboczi, E. J., Kushch, V. I., 2015. Computing elastic moduli on 3-D X-ray computed tomography image stacks. J. Mech. Phys. Solids 76, 84–97.

Ghossein, E., Levesque, M., 2012. A fully automated numerical tool for a comprehensive validation of homogenization models and its application to spherical particles reinforced composites. Int. J. Solids Struct. 49, 1387–1398.

Gilormini, P., Toulemonde, P.A., Diani, J., Gardere, A., 2017. Stress-strain response and volume change of a highly filled rubbery composite: experimental measurements and numerical simulations. Mech. Mater. 111, 57–65.

Gusev, A., 1997. Representative volume element size for elastic composites: A numerical study. J. Mech. Phys. Solids 45, 1449–1459.

Gusev, A., 2016. Controlled accuracy finite element estimates for the effective stiffness of composites with spherical inclusions. Int. J. Solids Struct. 80, 227–236.

Hazanov, S., Huet, C., 1994. Order relationships for boundary condition effects in heterogeneous bodies smaller than the representative volume. J. Mech. Phys. Solids 42, 1995–2011.

Hoover, W. G., Ree, F. H., 1968. Melting transition and communal entropy for hard spheres. J. of Chem. Phys. 49, 3609–3617.

Huet, C., 1990. Application of variational concepts to size effects in elastic heterogeneous bodies. J. Mech. Phys. Solids 38, 813–841.

Jodrey, W. S., Tory, E. M., 1985. Computer simulation of close random packing of equal spheres. Phys. Rev. A 32, 2347.

Kanit, T., Forest, S., Galliet, I., Mounoury, V., Jeulin, D., 2003. Determination of the size of the representative volume element for random composites: statistical and numerical approach. Int. J. Solids Struct. 40, 3647–3679.

Katzav, E., Berdichevsky, R., Schwartz, M., 2017. Random Close Packing and the Hard Sphere Percus-Yevick Theory. arXiv preprint arXiv:1703.09903.

Lee, H., Gillman, A. S., Matou, K., 2011. Computing overall elastic constants of polydisperse particulate composites from microtomographic data. J. Mech. Phys. Solids 59, 1838–1857.

Louis, P., Gokhale, A. M., 1995. Application of image analysis for characterization of spatial arrangements of features in microstructure. Metall. Mater. Trans. A 26, 1449–1456.

Lubachevsky, B. D., Stillinger, F. H., 1990. Geometric properties of random disk packings. J. Stat. Phys. 60, 561–583.

Maire, E., Fazekas, A., Salvo, L., Dendievel, R., Youssef, S., Cloetens, P., Letang, J. M., 2003. X-ray tomography applied to the characterization of cellular materials. Related finite element modeling problems. Compos. Sci. Technol. 63, 2431–2443.

Matlab, 2016. Matlab 2016a. MathWorks Inc.

McLaughlin, R., 1977. A study of the differential scheme for composite materials. Int. J. Eng. Sci. 15, 237–244.

Metropolis, N., Rosenbluth, A. W., Rosenbluth, M. N., Teller, A. H., Teller, E., 1953. Equation of state calculations by fast computing machines. J. Chem. Phys. 21, 1087–1092.

Moulinec, H., Suquet, P., 1998. A numerical method for computing the overall response of nonlinear composites with complex microstructure. Comput Methods Appl Mech Eng, 157, 69–94.

Ohser, J., and Schladitz, K., 2009. 3D images of materials structures: processing and analysis. John Wiley and Sons.

Park, K., Paulino,G. H.,2011. Cohesive zone models : a critical review of traction-separation relationship across fracture surfaces.Appl Mech Rev, 64.

Pathan, M. V., Tagarielli, V. L., Patsias, S., Baiz-Villafranca, P. M.,2017. A new algorithm to generate representative volume elements of composites with cylindrical or spherical fillers. Compos. Part B-Eng. 110, 267–278.

Reiss, H., Frisch, H., Lebowitz, J., 1959. Statistical mechanics of rigid spheres. J. Chem. Phys. 31, 369–380.

Reiss, H., 1992. Statistical geometry in the study of fluids and porous media. J. Phys. Chem. 96, 4736–4747.

Rintoul, M., Torquato, S., 1998. Hard-sphere statistics along the metastable amorphous branch. Phys. Rev. E 58, 532–537.

Rintoul, M. D., Torquato, S., 1996. Computer simulations of dense hard-sphere systems. J. Chem. Phys. 105, 9258–9265.

Robles, M., de Haro, M. L., Santos, A., 2014. Note: Equation of state and the freezing point in the hard-sphere model. J. Chem. Phys. 140, 136101.

Schberl, J., 1997. Netgen an advancing front 2D/3D-mesh generator based on abstract rules. Comput. Vis. Sci. 1, 41–52.

Schneider, K., Klusemann, B., Bargmann, S., 2016. Automatic three-dimensional geometry and mesh generation of periodic representative volume elements for matrix-inclusion composites. Adv. Eng. Softw. 99, 177–188.

Segurado, J., Llorca, J., 2002. A numerical approximation to the elastic properties of sphere-reinforced composites. J. Mech. Phys. Solids 50, 2107–2121.

Skoge, M., Donev, A., Stillinger, F. H., Torquato, S., 2006. Packing hyperspheres in high-dimensional euclidean spaces. Phys. Rev. E 74, 041127.

Tariel, V., Jeulin, D., Fanget, A., Contesse, G., 2011. 3D Multi-scale segmentation of granular materials. Image Anal. Stereol. 27, 23–28.

Tobochnik, J., Chapin, P. M., 1988. Monte Carlo simulation of hard spheres near random closest packing using spherical boundary conditions. J. Chem. Phys. 88, 5824–5830.

Torquato, S., 1991. Random heterogeneous media: Microstructure and improved bounds on effective properties. Appl. Mech. Rev. 44, 37–76.

Torquato, S., 1998. Effective stiffness tensor of composite media: II. Applications to isotropic dispersions. J. Mech. Phys. Solids 46, 1411–1440.

Torquato, S., 2002. Random heterogeneous materials: microstructure and macroscopic properties, Springer-Verlag, New York.

Torquato, S., Stell, G., 1985. Microstructure of two-phase random media. V. the n-point matrix probability functions for impenetrable spheres. J. Chem. Phys 82, 980–987.

Torquato, S., Lu, B., Rubinstein, J., 1990. Nearest-neighbor distribution functions in many-body systems. Phys. Rev. A 41, 2059–2075.

Torquato, S., Truskett, T. M., Debenedetti, P. G., 2000. Is random close packing of spheres well defined?. Phys. Rev. Lett. 84, 2064.

Van Loan, C., 1992. Computational frameworks for the fast Fourier transform. SIAM, Philadelphia.

Visscher, W. M., Bolsterli, M., 1972. Random Packing of Equal and Unequal Spheres in Two and Three Dimensions. Nature 239, 504–507.

Widom, B., 1966. Random sequential addition of hard spheres to a volume. J. Chem. Phys. 44, 3888–3894.

Williams, S. R., Philipse, A. P., 2003. Random packing of spheres and spherocylinders simulated by mechanical contraction. Phys. Rev. E 67, 1–9.

Yongshe, L., Yuanlin, J., Kyriakidis, P., 2006. Calculation of average covariance using fast Fourier transform (FFT). Stanford University, Menlo Park.